JACS ARTICLES

Published on Web 10/07/2010

A Hot Oxidant, 3-NO_2Y_{122} Radical, Unmasks Conformational Gating in Ribonucleotide Reductase

Kenichi Yokoyama,[†] Ulla Uhlin,[§] and JoAnne Stubbe*[,†,‡]

Departments of Chemistry and Biology, Massachusetts Institute of Technology, 77 Massachusetts Avenue, Cambridge, Massachusetts 02139-4307, United States, and Department of Molecular Biology, Swedish University of Agricultural Science, Uppsala Biomedical Center, Box 590, SE-75124 Uppsala, Sweden

Received August 3, 2010; E-mail: stubbe@mit.edu

Abstract: *Escherichia coli* ribonucleotide reductase is an $\alpha 2\beta 2$ complex that catalyzes the conversion of nucleotides to deoxynucleotides and requires a diferric-tyrosyl radical ($Y^{\bullet}$) cofactor to initiate catalysis. The initiation process requires long-range proton-coupled electron transfer (PCET) over 35 Å between the two subunits by a specific pathway ($Y_{122}^{\bullet} \rightarrow W_{48} \rightarrow Y_{356}$ within β to $Y_{731} \rightarrow Y_{730} \rightarrow C_{439}$ within α). The rate-limiting step in nucleotide reduction is the conformational gating of the PCET process, which masks the chemistry of radical propagation. 3-Nitrotyrosine (NO_2Y) has recently been incorporated site-specifically in place of Y_{122} in $\beta 2$. The protein as isolated contained a diferric cluster but no nitrotyrosyl radical ($NO_2Y^{\bullet}$) and was inactive. In the present paper we show that incubation of apo-$Y_{122}NO_2Y$-$\beta 2$ with Fe^{2+} and O_2 generates a diferric-$NO_2Y^{\bullet}$ that has a half-life of 40 s at 25 °C. Sequential mixing experiments, in which the cofactor is assembled to 1.2 $NO_2Y^{\bullet}/\beta 2$ and then mixed with $\alpha 2$, CDP, and ATP, have been analyzed by stopped-flow absorption spectroscopy, rapid freeze quench EPR spectroscopy, and rapid chemical quench methods. These studies have, for the first time, unmasked the conformational gating. They reveal that the $NO_2Y^{\bullet}$ is reduced to the nitrotyrosinate with biphasic kinetics (283 and 67 s^{-1}), that dCDP is produced at 107 s^{-1}, and that a new $Y^{\bullet}$ is produced at 97 s^{-1}. Studies with pathway mutants suggest that the new $Y^{\bullet}$ is predominantly located at 356 in $\beta 2$. In consideration of these data and the crystal structure of $Y_{122}NO_2Y$-$\beta 2$, a mechanism for PCET uncoupling in $NO_2Y^{\bullet}$-RNR is proposed.

Introduction

Ribonucleotide reductases (RNRs) catalyze the conversion of ribonucleotides to deoxyribonucleotides in all organisms. The class Ia RNRs are composed of two subunits: α, where nucleotide reduction occurs and allosteric effectors bind to control substrate specificity and overall reactivity, and β, where the essential diferric-tyrosyl radical ($Y^{\bullet}$) cofactor resides.[1−3] The *Escherichia coli* RNR is active as an $\alpha 2\beta 2$ complex, and nucleotide reduction is initiated by a long-range proton-coupled electron transfer (PCET) process in which $Y_{122}^{\bullet}$ in $\beta 2$ reversibly oxidizes C_{439} in α to a thiyl radical through a proposed pathway ($Y_{122} \rightarrow W_{48} \rightarrow Y_{356}$ within β to $Y_{731} \rightarrow Y_{730} \rightarrow C_{439}$ within α, Figure 1).[4,5] Our studies have shown that this process is masked by a rate-limiting conformational change (or changes) and that the conformational change is initiated by the binding of the substrate and allosteric effector to α.[6−9] Conformational changes thus mask the PCET process. Recently we have incorporated 3-nitrotyrosine (NO_2Y) site-specifically in place of each Y in the pathway.[10] Incorporation of NO_2Y in place of Y_{122} in β revealed an assembled diferric cluster with no 3-nitrotyrosine radical ($NO_2Y^{\bullet}$). In the present paper we demonstrate that this $NO_2Y^{\bullet}$ can be formed but has a $t_{1/2}$ at 25 °C of 40 s. This $t_{1/2}$ is sufficiently long for analysis of the catalytic properties of this mutant RNR by sequential mixing, pre-steady-state experiments using stopped-flow (SF) absorption spectroscopy, rapid chemical quench (RCQ) methods, and rapid freeze quench (RFQ) methods in liquid isopentane. These studies together reveal uncoupling of the conformational gating and the first step in the propagation process (Figure 1), providing direct chemical insight into specific steps in the pathway.

Electron transfer (ET) in biological systems has been studied in detail using artificial electron donors or acceptors with small model proteins, where conformational gating has been minimized.[11] The general rules governing this ubiquitous process are well understood. However, in RNR, the oxidation of C_{439}-α is proposed to occur over a 35 Å distance[4] and requires

[†] Department of Chemistry, Massachusetts Institute of Technology.
[‡] Department of Biology, Massachusetts Institute of Technology.
[§] Department of Molecular Biology, Swedish University of Agricultural Science.

(1) Stubbe, J.; van der Donk, W. A. *Chem. Rev.* **1998**, *98*, 705–762.
(2) Jordan, A.; Reichard, P. *Annu. Rev. Biochem.* **1998**, *67*, 71–98.
(3) Nordlund, P.; Reichard, P. *Annu. Rev. Biochem.* **2006**, *75*, 681–706.
(4) Uhlin, U.; Eklund, H. *Nature* **1994**, *370*, 533–539.
(5) Stubbe, J.; Nocera, D.; Yee, C. S.; Chang, M. C. Y. *Chem. Rev.* **2003**, *103*, 2167–2201.
(6) Ge, J.; Yu, G.; Ator, M. A.; Stubbe, J. *Biochemistry* **2003**, *42*, 10071–10083.
(7) Seyedsayamdost, M. R.; Xie, J.; Chan, C. T.; Schultz, P. G.; Stubbe, J. *J. Am. Chem. Soc.* **2007**, *129*, 15060–15071.
(8) Seyedsayamdost, M. R.; Yee, C. S.; Reece, S. Y.; Nocera, D. G.; Stubbe, J. *J. Am. Chem. Soc.* **2006**, *128*, 1562–1568.
(9) Seyedsayamdost, M. R.; Stubbe, J. *J. Am. Chem. Soc.* **2006**, *128*, 2522–2523.
(10) Yokoyama, K.; Uhlin, U.; Stubbe, J. *J. Am. Chem. Soc.* **2010**, *132*, 8385–8397.
(11) Gray, H. B.; Winkler, J. R. *Q. Rev. Biophys.* **2003**, *36*, 341–372.

10.1021/ja1069344

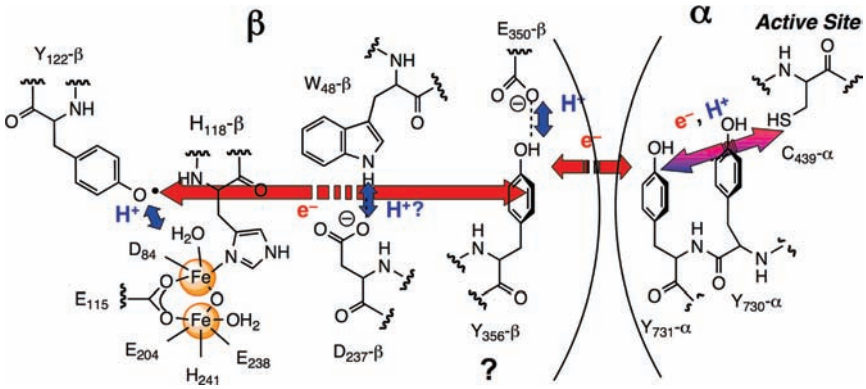

Figure 1. Proposed PCET pathway in *E. coli* class Ia RNR. Red and blue arrows indicate orthogonal transfer of the electron and proton, respectively. The purple arrow indicates collinear movement of the electron and proton. Y_{356}- and E_{350}-β2 are in the flexible C-terminal tail and are disordered in all crystal structures.

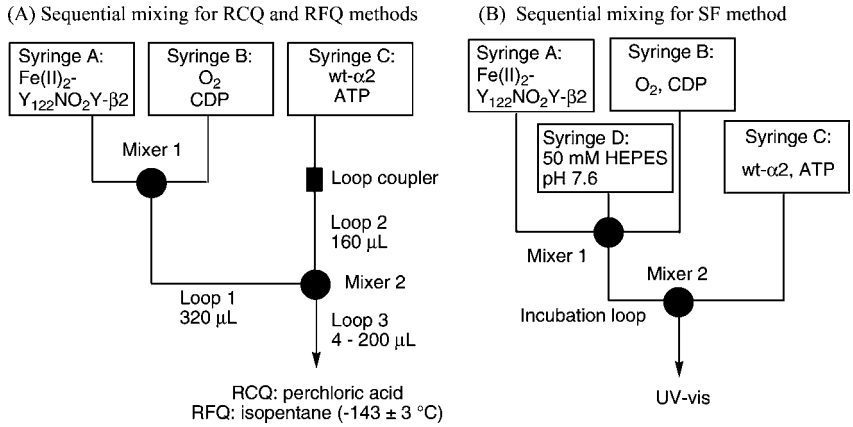

Figure 2. Schematic representation of the sequential mixing setups for (A) RCQ and RFQ experiments and (B) SF experiments. Details are described in Materials and Methods.

intermediates to account for the turnover numbers of 2−10 s^{-1} with different substrate/effector (S/E) pairs.[5,12] Redox-active amino acids are proposed to function in this capacity.[4,5,12−14] Our previous studies with NO_2Y-RNRs with NO_2Y incorporated in place of Y_{356}, Y_{730}, or Y_{731} revealed that these mutants are unable to support dNDP formation,[10] likely the result of the inability of $Y^\bullet$ to oxidize this residue (unfavorable by 200 mV at pH 7).[15] However, NO_2Y at 122 is distinct from the other NO_2Y's in the pathway, as it can potentially be oxidized by an Fe^{4+}/Fe^{3+} species (intermediate X)[16,17] involved in active cluster assembly. The proposed mechanism of Y_{122} oxidation is that the proton from its phenol is transferred to the hydroxyl bound to Fe1 of the cluster (Figure 1).[5,17,18] Typically, 1.2 $Y^\bullet$/β2 are obtained by this self-assembly process in vitro.[19] Whether intermediate X is a sufficiently potent oxidant to oxidize NO_2Y_{122} was unknown. In addition, studies from the Sjöberg laboratory have shown that mutations in the vicinity of the diferric-$Y^\bullet$ cofactor often result in formation of a $Y^\bullet$ with greatly reduced stability relative to the $Y^\bullet$ in wt-β2 ($t_{1/2}$ of seconds to minutes vs 4 days, respectively).[20] The inability to detect $NO_2Y_{122}{}^\bullet$ in our initial experiments could thus be related to the inability of X to oxidize NO_2Y or a short $t_{1/2}$. $NO_2Y^\bullet$, if generated, is a potent oxidant[15] and could potentially oxidize residues within the pathway (Figure 1) and lead to dNDP production.

The present paper demonstrates that $NO_2Y^\bullet$ can be formed and that it has a sufficiently long $t_{1/2}$ to investigate its chemical reactivity. To carry out these experiments, a general sequential mixing protocol on the millisecond time scale was used, as described in Figure 2. In this protocol, $Y_{122}NO_2Y$-β2 is preloaded under anaerobic conditions with Fe^{2+} and then is mixed with cytidine 5′-diphosphate (CDP) and O_2 for a time period to maximize the amount of $NO_2Y^\bullet$ (1 s). This solution is then mixed with a third solution containing α and allosteric effector adenosine triphosphate (ATP), and the reaction is monitored from 10 to 200 ms by three methods: SF visible absorption spectroscopy, RCQ followed by radioactive quantitation of dCDP formation, and RFQ in liquid isopentane followed by electron paramagnetic resonance (EPR) analysis. Analysis of the kinetic data reveals that $NO_2Y^\bullet$ is reduced to nitrophenolate with rate constants of 283 and 67 s^{-1}, that dCDP

(12) Reece, S. Y.; Hodgkiss, J. M.; Stubbe, J.; Nocera, D. G. *Phil. Trans. R. Soc. B* **2006**, *361*, 1351–1364.
(13) Ekberg, M.; Sahlin, M.; Eriksson, M.; Sjöberg, B.-M. *J. Biol. Chem.* **1996**, *271*, 20655–20659.
(14) Climent, I.; Sjöberg, B.-M.; Huang, C. Y. *Biochemistry* **1992**, *31*, 4801–4807.
(15) Yee, C. S.; Seyedsayamdost, M. R.; Chang, M. C.; Nocera, D. G.; Stubbe, J. *Biochemistry* **2003**, *42*, 14541–14552.
(16) Bollinger, J. M., Jr.; Edmondson, D. E.; Huynh, B. H.; Filley, J.; Norton, J. R.; Stubbe, J. *Science* **1991**, *253*, 292–298.
(17) Sturgeon, B. E.; Burdi, D.; Chen, S.; Huynh, B. H.; Edmondson, D.; Stubbe, J.; Hoffman, B. *J. Am. Chem. Soc.* **1996**, *118*, 7551–7557.
(18) Shanmugam, M.; Doan, P. E.; Lees, N. S.; Stubbe, J.; Hoffman, B. M. *J. Am. Chem. Soc.* **2009**, *131*, 3370–3376.
(19) Tong, W. H.; Chen, S.; Lloyd, S. G.; Edmondson, D. E.; Huynh, B. H.; Stubbe, J. *J. Am. Chem. Soc.* **1997**, *118*, 2107–2108.
(20) Ormo, M.; Regnstrom, K.; Wang, Z.; Que, L., Jr.; Sahlin, M.; Sjoberg, B. M. *J. Biol. Chem.* **1995**, *270*, 6570–6576.

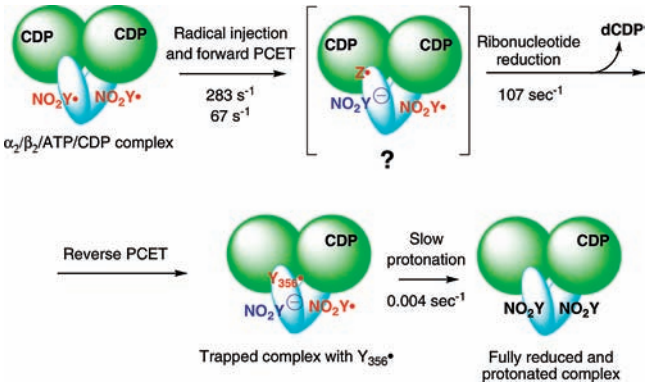

Figure 3. Model for the reaction of $Y_{122}NO_2Y$-$\beta2$ with α2, ATP and CDP. Green circles represent α, and blue ovals, β. The ATP allosteric effector is omitted from α for clarity. There are 1.2 $NO_2Y^{\bullet}/\beta2$, not 2 as shown in the figure, and their distribution in $\beta2$ is not understood. Any intermediate(s) between the forward PCET and ribonucleotide reduction is (are) designated as $Z^{\bullet}$.

is generated with an apparent rate constant of 107 s^{-1}, and that a new radical, likely located at residue 356 in $\beta2$, is generated with an apparent rate constant of 97 s^{-1}. The results suggest for the first time that some or all of the conformational gating has been removed by the uncoupling of the proton and electron transfer in the reduction of the $NO_2Y^{\bullet}$. The X-ray crystal structure of $Y_{122}NO_2Y$-$\beta2$, refined to 2.2 Å, is presented and used to propose a mechanism(s) for PCET uncoupling at Y_{122}. These studies have resulted in the model shown in Figure 3 that will be presented in detail.

Materials and Methods

Luria−Bertani (LB) medium, BactoAgar, and 100 mm Petri dish plates were obtained from Becton-Dickinson. NO_2Y, M9 salts, ampicillin (Amp), L-arabinose (LAra), chloramphenicol (Cm), all amino acids, ATP, CDP, NADPH, ethylenediamine tetraacetic acid (EDTA), Bradford Reagent, Sephadex G-25, phenylmethanesulfonyl fluoride (PMSF), and streptomycin sulfate were purchased from Sigma-Aldrich. Isopropyl β-D-thiogalactopyranoside (IPTG) and dithiothreitol (DTT) were from Promega. *E. coli* TOP10 competent cells were from Invitrogen. Calf-intestine alkaline phosphatase (CIAP, 20 U/μL) was from Roche. [5-^{3}H]CDP was purchased from ViTrax (Placentia, CA). Calibrated EPR tubes (3.2 ± 0.01 and 2.8 ± 0.01 mm inner diameter for RFQ and hand-quench experiments, respectively) were from Wilmad Labglass (Vineland, NJ). The purification of *E. coli* thioredoxin[21] (TR, 40 units/mg), *E. coli* thioredoxin reductase[22] (TRR, 1400 units/mg), wt-$\beta2$[23] (6200−7500 nmol min^{-1} mg^{-1}, 1.1−1.2 radicals/$\beta2$), and wt-α2[24] (2500−3000 nmol min^{-1} mg^{-1}) have previously been described. The concentration of α2 was determined using ε_{280nm} = 189 mM^{-1} cm^{-1}.[25] Wild-type (wt) and all mutant α2's were pre-reduced by DTT and treated with hydroxyurea (HU) to reduce any $Y^{\bullet}$ in endogenous β that copurifies, following the reported procedure,[7] and exchanged to assay buffer (50 mM HEPES (titrated with NaOH), 15 mM $MgSO_4$, 1 mM EDTA, pH 7.6). The concentrations of $\beta2$ and $Y_{122}NO_2Y$-$\beta2$ were determined using ε_{280nm} = 131 mM^{-1} cm^{-1}.[25] The concentration of apo-$Y_{122}NO_2Y$-$\beta2$ was determined using ε_{280nm} = 120 mM^{-1} cm^{-1}.[26] The amino acid enriched glycerol minimal media leucine (GMML) and heavy metal stock solution (1000×) have previously been described.[27,28] UV−vis absorption spectra were determined using a Cary 3 UV−vis spectrophotometer (Varian, Walnut Creek, CA), and an Ultramark EX microplate imaging system (BioRad) was used to monitor fractions from column chromatography: A_{280nm} for protein and A_{340nm} for the diferric cluster and NO_2Y phenol. RFQ and RCQ experiments were carried out using an Update Instruments 1019 syringe ram unit and a model 715 syringe ram controller. For RFQ experiments, the samples were sprayed into a funnel containing liquid isopentane at −143 ± 3 °C. The temperature was maintained by its placement in a liquid isopentane bath with a liquid N_2 jacket. The temperature was monitored using a Fluke 52 dual-input thermometer with an Anritsu Cu thermocouple probe. Nonlinear least-squares fitting of kinetic data was carried out using KaleidaGraph software (Synergy Software, Reading, PA). EPR spin quantitation was carried out using Cu(II)SO_4 as a standard.[29]

Expression and Purification of $Y_{122}NO_2Y$-$\beta2$. A plasmid coding for untagged β with a TAG codon at amino acid position 122, pBAD-*nrdB*($Y_{122}Z$), was prepared from pBAD-*nrdB*[30] using previously reported primers and PCR conditions.[10] $Y_{122}NO_2Y$-$\beta2$ was expressed in *E. coli* TOP10 cells harboring pEVOL-NO_2Y[10,31] and pBAD-*nrdB*($Y_{122}Z$) grown in the amino acid enriched GMML medium[27] and was purified using DEAE and Q-sepharose column chromatography as previously described.[10] Typically, 20 mg of $NO_2Y^{\bullet}$ reduced (met)-$Y_{122}NO_2Y$-$\beta2$ (3.0 ± 0.2 Fe/$\beta2$, 2.0 ± 0.1 $NO_2Y/\beta2$, <0.1 radicals/$\beta2$) was isolated from 1 g of cell paste. Apo-$Y_{122}NO_2Y$-$\beta2$ (<0.1 Fe/$\beta2$) was prepared using hydroxyquinoline as a chelator in the presence of 1 M imidazole.[26] The iron content was determined by the ferrozine assay.[32]

Preparation of Y_{122}[β-$^2H_2$]NO_2Y-$\beta2$. Y_{122}[β-$^2H_2$]NO_2Y-$\beta2$ was expressed and purified as described above using [β-$^2H_2$]NO_2Y in place of NO_2Y. [β-$^2H_2$]NO_2Y was prepared by nitration of [β-$^2H_2$]Y (98 atom % ^{2}H).[33] The deuterium incorporation was >96% based on ^{1}H NMR analysis. ^{1}H NMR (300 MHz, D_2O, 25 °C): δ = 4.24 (s, 1H, Cα-H), 7.13 (d, 1H, arom. C−H, J = 8.7 Hz), 7.52 (dd, 1H, arom. C−H, J = 2.2 Hz, 8.7 Hz), 8.01 (d, 1H, arom. C−H, J = 2.2 Hz). ^{13}C NMR (75 MHz, D_2O, 25 °C) δ = 34.7 (s, Cβ), 54.2 (s, Cα), 120.4 (d, arom. C2, J = 2.1 Hz), 126.1 (d, arom. C1, J = 1.6 Hz), 126.8 (d, arom. C4, J = 2.4 Hz), 134.2 (d, arom. C3, J = 15.2 Hz), 138.2 (s, arom. C6), 153.1 (d, arom. C5, J = 1.15 Hz), 172.1 (s, COOH). UV−vis absorption: in 50 mM MES, pH 5.0, λ_{max} 360 nm (ε = 3000 ± 100 M^{-1} cm^{-1}); in 50 mM TAPS, pH 9.0, λ_{max} 424 nm (ε = 4500 ± 100 M^{-1} cm^{-1}).

Expression and Purification of $Y_{122}NO_2Y/Y_{356}F$-$\beta2$. The $Y_{356}F$ mutation was introduced by PCR using pBAD-*nrdB*($Y_{122}Z$) as a template, forward primer $Y_{356}F$-f (5′-GTG GAA GTC AGT TCT TTT CTG GTC GGG CAG ATT GAC-3′), and reverse primer $Y_{356}F$-r (5′-GTC AAT CTG CCC GAC CAG AAA AGA ACT GAC TTC CAC-3′). PCR was performed using PfuUltraII polymerase (Stratagene) for 18 cycles following the manufacturer's protocol with an annealing temperature of 55 °C. The methylated template was then digested by *Dpn*I. The mutation was confirmed by sequencing at the MIT Biopolymers Laboratory. The expression and purification of $Y_{122}NO_2Y/Y_{356}F$-$\beta2$ were performed as described for $Y_{122}NO_2Y$-$\beta2$. Typically, 20 mg of protein was isolated per gram of cell paste.

(21) Chivers, P. T.; Prehoda, K. E.; Volkman, B. F.; Kim, B. M.; Markley, J. L.; Raines, R. T. *Biochemistry* **1997**, *36*, 14985–14991.
(22) Pigiet, V. P.; Conley, R. R. *J. Biol. Chem.* **1977**, *252*, 6367–6372.
(23) Salowe, S. P.; Stubbe, J. *J. Bacteriol.* **1986**, *165*, 363–366.
(24) Salowe, S. P.; Ator, M. A.; Stubbe, J. *Biochemistry* **1987**, *26*, 3408–3416.
(25) Thelander, L. *J. Biol. Chem.* **1973**, *248*, 4591–4601.
(26) Atkin, C. L.; Thelander, L.; Reichard, P.; Lang, G. *J. Biol. Chem.* **1973**, *248*, 7464–7472.
(27) Hammill, J. T.; Miyake-Stoner, S.; Hazen, J. L.; Jackson, J. C.; Mehl, R. A. *Nat. Protoc.* **2007**, *2*, 2601–2607.
(28) Farrell, I. S.; Toroney, R.; Hazen, J. L.; Mehl, R. A.; Chin, J. W. *Nat. Methods* **2005**, *2*, 377–384.
(29) Palmer, G. *Methods Enzymol.* **1967**, *10*, 595.
(30) Hristova, D.; Wu, C. H.; Jiang, W.; Krebs, C.; Stubbe, J. *Biochemistry* **2008**, *47*, 3989–3999.
(31) Young, T. S.; Ahmad, I.; Yin, J. A.; Schultz, P. G. *J. Mol. Biol.* **2010**, *395*, 361–374.
(32) Fish, W. W. *Methods Enzymol.* **1988**, *158*, 357–364.
(33) Seyedsayamdost, M. R.; Argirević, T.; Minnihan, E. C.; Stubbe, J.; Bennati, M. *J. Am. Chem. Soc.* **2009**, *131*, 15729–15738.

In Vitro Reconstitution of $NO_2Y^{\bullet}$−Diferric Cluster and Characterization by EPR Spectroscopy. Apo-$Y_{122}NO_2Y$-β2 (100 μM) in 0.5 mL of 50 mM HEPES (pH 7.6) was degassed on a Schlenk line by 15 cycles of 10 s evacuation, followed by 2 min of Ar gas refill. The sample was then brought into a glovebox and incubated with 5 equiv of $Fe^{II}(NH_4)_2(SO_4)_2$ at 4 °C for 5−10 min. $[Fe(II)]_2$-$Y_{122}NO_2Y$-β2 (0.3 mL) was transferred to a glass vial sealed with a septum, taken out of the glovebox, and quickly mixed with an equal volume of O_2-saturated (1.4 mM) 50 mM HEPES (pH 7.6) to a final concentration of 50 μM $[Fe(II)]_2$-$Y_{122}NO_2Y$-β2 (5 Fe^{2+}/β2) and 0.7 mM O_2. The mixture was incubated for 20 s at 25 °C before quenching in liquid N_2. The reconstitution of $Y_{122}[\beta$-$^2H_2]NO_2Y$-β2 was carried out in an identical fashion. EPR spectra were recorded at 77 K in the MIT Department of Chemistry Instrumentation Facility on a Bruker ESP-300 X-band spectrometer equipped with a quartz finger dewar filled with liquid N_2. EPR parameters: microwave frequency, 9.34 GHz; power, 30 μW; modulation amplitude, 1.5 G; modulation frequency, 100 kHz; time constant, 5.12 ms; scan time, 41.9 s. Spectral simulation and fitting were performed using EasySpin.[34] The *g*-values, hyperfine coupling constants, and Euler angles for $Y_{122}^{\bullet}$ in wt-β2 were used as the starting parameters, and least-squares fitting was performed by varying the aforementioned parameters and the line width. For the microwave power saturation experiment, the EPR spectra were recorded as a function of microwave power, and the integrated intensity of each signal was plotted against the square root of power. The resulting data were fit to eq 1,[35,36]

$$\text{signal amplitude} = K(P^{0.5})/[1 + (P/P_{1/2})]^{0.5b} \qquad (1)$$

where K is a sample- and instrument-dependent scaling factor, P is the microwave power, b is indicative of homogeneous ($b = 3$) or inhomogeneous ($b = 1$) spectral broadening, and $P_{1/2}$ is the microwave power at half-saturation of the EPR signal.

Analysis of $NO_2Y^{\bullet}$ Formation and Decay by RFQ-EPR. $[Fe(II)]_2$-$Y_{122}NO_2Y$-β2 (60 μM, 5 Fe^{2+}/β2) in anaerobic 50 mM HEPES (pH 7.6) in one syringe, prepared as described above, was mixed with O_2-saturated 50 mM HEPES (pH 7.6) in the second syringe in a 1:1 ratio at 25 °C and aged for a pre-determined time period (0.5−50 s) in the reaction loop. The mixture (400 μL) was then sprayed, by actuation of the ram drive at a velocity of 1.25 cm/s,[37] into liquid isopentane (−143 ± 3 °C) in a glass funnel attached to an EPR tube. The frozen sample was then packed into the EPR tube using a stainless steel packer and stored in liquid N_2 until the EPR spectrum was acquired. A packing factor of 0.64 ± 0.02 was reproducibly obtained with wt-β2 samples.[37,38]

Determination of the Absorption Spectrum of the $NO_2Y_{122}^{\bullet}$ in $Y_{122}NO_2Y$-β2 Using SF Absorption Spectroscopy and Decomposition of Superimposed Spectra. SF kinetics were carried out on an Applied Photophysics DX 17MV instrument equipped with the Pro-Data upgrade using PMT detection. The temperature was maintained at 25 ± 1 °C with a Lauda RE106 circulating water bath. The circulating water contained ~10 mM sodium dithionite to minimize O_2 diffusion into the SF lines. Prior to the experiment, the SF lines were washed with 10 mL of a 500 mM sodium dithionite solution, 30 mL of anaerobic water, and 10 mL of anaerobic 50 mM HEPES (pH 7.6). The connections of the SF syringes to the instrument were purged with N_2 throughout the experiments. $[Fe(II)]_2$-$Y_{122}NO_2Y$-β2 (60 μM, 5 Fe^{II}/β2) in anaerobic 50 mM HEPES (pH 7.6) in one syringe was mixed with O_2-saturated 50 mM HEPES (pH 7.6) in a 1:1 ratio. The reaction was monitored from 320 to 550 nm in 10 nm intervals, four traces were averaged at each wavelength, and the spectra were reconstructed. For the following analysis to deconvolute the absorption spectrum of $NO_2Y^{\bullet}$, the 0.44 s time point, at which the amount of $NO_2Y^{\bullet}$ is maximized, was chosen. From this spectrum, 2.0 equiv of diferric cluster[16] and 0.8 equiv of NO_2Y phenol[10] were subtracted. The amount of diferric cluster was based on the Fe content (4.0/β2) in met-$Y_{122}NO_2Y$-β2 isolated after in vitro reconstitution. The amount of NO_2Y phenol was determined by subtracting the amount of $NO_2Y^{\bullet}$ (1.2/β2) determined by RFQ-EPR spectroscopy from the amount of total NO_2Y (2.0/β2), assuming that the amount of NO_2Y phenolate (NO_2Y^-) was negligible (<0.03/β2) based on the absorption at 450 nm.[10] The resulting spectrum (Figure 4) is that of the $NO_2Y^{\bullet}$.

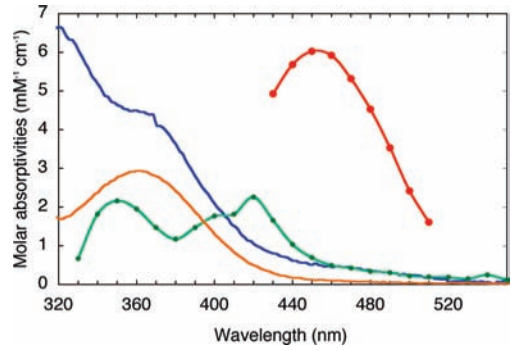

Figure 4. UV−vis absorption spectra of the species contributing to the SF UV−vis composite absorption spectrum generated from the reaction between Fe^{II}−$Y_{122}NO_2Y$-β2 and O_2 and the reaction of $Y_{122}NO_2Y^{\bullet}$-β2 with α2, ATP, and CDP: diferric cluster, blue; NO_2Y_{122} phenol, orange; $NO_2Y_{122}^-$, red; and $NO_2Y^{\bullet}$, green. See Materials and Methods for the details of the spectral reconstructions.

Activity Assay of $Y_{122}NO_2Y$-β2 with wt-α2, ATP, and CDP ± TR/TRR/NADPH. All reactions were carried out at 25 °C. $[Fe(II)]_2$-$Y_{122}NO_2Y$-β2 (100 μM, 5 Fe^{II}/β2) in anaerobic 50 mM HEPES (pH 7.6, 90 μL) was mixed with O_2-saturated 50 mM HEPES (pH 7.6) containing [5-^{3}H]CDP (3000−5000 cpm/nmol, 5 mM, 90 μL) and incubated for 7 ± 2 s to generate 0.95 ± 0.05 $NO_2Y^{\bullet}/\beta$2. This solution (180 μL) was then mixed with wt-α2 and ATP in 1.7× assay buffer (270 μL) to give a final volume of 450 μL, containing 20 μM $Y_{122}NO_2Y$-β2 and α2, 3 mM ATP, and 1 mM [5-^{3}H]CDP. Aliquots (80 μL) were removed from 10 to 40 s, and the reaction was quenched by the addition of 2% perchloric acid (50 μL). The reactions were subsequently neutralized with 40 μL of 0.5 M KOH. Each sample was then incubated at −20 °C for 6−12 h to ensure complete precipitation of potassium perchlorate. The protein was then removed by centrifugation for 3 min using a tabletop centrifuge. Each supernatant was transferred to a 1.5 mL microfuge tube, to which 7 U of CIAP, 120 nmol of carrier deoxycytidine (dC), and 0.15 mM EDTA in 75 mM Tris buffer (pH 8.5) were added. The amount of dC was analyzed by the method of Steeper and Steuart.[39] The experiment was also carried out in the presence of TR (30 μM)/TRR (0.5 μM)/NADPH (1 mM).

Kinetics of dCDP Formation Monitored by the RCQ Method. Sequential mixing RCQ and RFQ experiments were carried out by the following general procedure using three syringes and an Update Instrument 1019 syringe ram unit following the manufacturer's protocol (Figure 2A). Ram drive velocities of 1.25 and 1.0 cm/s were used for the first and the second pushes, respectively. The ram drive pushes all three syringes simultaneously. Loops 1, 2, and 3 were initially filled with 50 mM HEPES (pH 7.6). All reactions were carried out at 25 °C. $[Fe(II)]_2$-$Y_{122}NO_2Y$-β2 (60 μM, 5 Fe^{II}/β2) in syringe A was first mixed with an equal volume of an O_2-saturated 50 mM HEPES (pH 7.6) containing [5-^{3}H]CDP

(34) Stoll, S.; Schweiger, A. *J. Magn. Reson.* **2006**, *178*, 42–55.
(35) Chen-Barrett, Y.; Harrison, P. M.; Treffry, A.; Quail, M. A.; Arosio, P.; Santambrogio, P.; Chasteen, N. D. *Biochemistry* **1995**, *34*, 7847–7853.
(36) Sahlin, M.; Petersson, L.; Graslund, A.; Ehrenberg, A.; Sjoberg, B. M.; Thelander, L. *Biochemistry* **1987**, *26*, 5541–5548.
(37) Ballou, D. P. *Methods Enzymol.* **1978**, *54*, 85–93.
(38) Bollinger, J. M., Jr.; Tong, W. H.; Ravi, N.; Huynh, B. H.; Edmondson, D. E.; Stubbe, J. A. *Methods Enzymol.* **1995**, *258*, 278–303.
(39) Steeper, J. R.; Steuart, C. D. *Anal. Biochem.* **1970**, *34*, 123–130.

(3000−5000 cpm/nmol, 3 mM) from syringe B to replace 95% of loop 1 content (300 μL, Figure 2A) and aged for 1 s to allow maximum production of the $NO_2Y^\bullet$ (1.2 ± 0.05 equiv/β2). The push also replaced 95% of loop 2 content with 150 μL of wt-α2 (60 μM) and ATP (9 mM) in 3× assay buffer from syringe C. The contents of loop 1 (300 μL) and loop 2 (150 μL) were then mixed by the second push and aged for 0.01−0.20 s by traversing loop 3. The final reaction mixture contained 20 μM $Y_{122}NO_2Y$-β2 and α2, 3 mM ATP, and 1 mM [5-^{3}H]CDP in assay buffer. This mixture (450 μL) was then sprayed into 350 μL of cold 2% perchloric acid. After each run, the mixture was neutralized with 300 μL of 0.5 M KOH and stored at −20 °C for 6−12 h. The workup was identical to that described in the previous section.[39] The rate constants were obtained by a nonlinear least-squares fit of the dCDP formation data to eq 2,

$$y = A_1(1 - e^{-k_1 t}) + A_2(1 - e^{-k_2 t}) \quad (2)$$

where t is time (s), y is dCDP concentration at t, A_1 and A_2 are the amplitudes, and k_1 and k_2 are the rate constants for each kinetic phase. y and t are experimentally determined, and A_1, A_2, k_1, and k_2 are obtained from the fitting.

Kinetics of NO_2Y^- Formation during the Reaction of $Y_{122}NO_2Y$-β2 with wt-α2, ATP, and CDP Monitored by SF Absorption Spectroscopy. All reactions were carried out at 25 °C. An Applied Photophysics instrument was reconfigured for sequential mixing following the manufacturer's protocol (Figure 2B). The instrument allows movement of syringes A and B independently from syringes C and D. [Fe(II)]$_2$-$Y_{122}NO_2Y$-β2 (80 μM, 5 Fe^{2+}/β2) in anaerobic 50 mM HEPES (pH 7.6) in syringe A was mixed with an equal volume of O_2-saturated 50 mM HEPES (pH 7.6) containing CDP (4 mM) in syringe B and aged for 1 s to maximize $NO_2Y^\bullet$ formation in the incubation loop. The resulting solution was then mixed with equal volumes of wt-α2 (40 μM) and ATP (6 mM) in 2× assay buffer using syringes C and D. The final reaction mixture contained 20 μM $Y_{122}NO_2Y$-β2 and α2, 3 mM ATP, and 1 mM CDP in assay buffer. The reaction was monitored at 460 nm, and 15 traces were averaged. For the point-by-point reconstruction of the absorption spectrum, the reaction was monitored from 390 to 510 nm in 10 nm intervals, and 2−5 traces were averaged at each wavelength. The rate constants were obtained by a nonlinear least-squares fit of the SF trace at A_{460nm} to eq 3,

$$y = A_1(1 - e^{-k_1 t}) + A_2(1 - e^{-k_2 t}) + A_3(1 - e^{-k_3 t}) \quad (3)$$

where the parameters are as described above.

Determination of the Absorption Spectrum of the $NO_2Y_{122}^-$ in $Y_{122}NO_2Y$-β2 Using SF Absorption Spectroscopy and Decomposition of Superimposed Spectra. The $NO_2Y_{122}^-$ spectrum was obtained from the spectra generated by the SF method during the reaction of $Y_{122}NO_2Y$-β2 with wt-α2, ATP, and CDP. The spectrum from the 2 ms time point was subtracted from that at 120 ms. The region between 430 and 510 nm, where the spectrum overlaps minimally with other species, was determined. The extinction coefficient was calculated by assuming that the amount of $NO_2Y^\bullet$ reduced in this period of time corresponds to the amount of NO_2Y^- and the amount of $NO_2Y^\bullet$ reduced, as determined by RFQ-EPR described subsequently.

Kinetics of $NO_2Y^\bullet$ Reduction and Formation of a New Radical Monitored by RFQ-EPR Spectroscopy. Sequential mixing experiments were carried out as described above for RCQ except that the quenching occurred by spraying the sample into isopentane (Figure 2B). [Fe(II)]$_2$-$Y_{122}NO_2Y$-β2 or [Fe(II)]$_2$-Y_{122}[β-$^2H_2$]NO_2Y-β2 (90 μM, 5 Fe^{2+}/β2) in anaerobic 50 mM HEPES (pH 7.6) was mixed with an equal volume of O_2-saturated 50 mM HEPES (pH 7.6) containing CDP (3 mM) and aged for 1 s at 25 °C. This solution (300 μL) was then mixed with 150 μL of a solution containing wt-α2 (90 μM) and ATP (9 mM) in 3× assay buffer and aged for 0.01−0.20 s. The final reaction mixture contained 30 μM $Y_{122}NO_2Y$-β2 or Y_{122}[β-$^2H_2$]NO_2Y-β2, 30 μM α2, 3 mM ATP, and 1 mM CDP in assay buffer. The reaction was quenched and packed into an EPR tube. The packing factor of wt-α2β2 complex was determined to be 0.52 ± 0.02. EPR spectra were collected as described above for $NO_2Y^\bullet$.

The EPR spectra of the new radical and the $NO_2Y^\bullet$ overlap extensively. The low-field region of the composite spectrum was initially used to estimate the amount of the new radical. To actually obtain the spectrum of the new radical, however, experiments with both $Y_{122}NO_2Y$- and with Y_{122}[β-$^2H_2$]NO_2Y-β2 were carried out. The assumption was made that both proteins give rise to the same radical species in the same amounts. A spectrum of $NO_2Y^\bullet$ and [β-$^2H_2$]$NO_2Y^\bullet$ was then independently subtracted from the composite spectrum. The amount subtracted was continually readjusted to minimize the differences between the spectrum of the new species obtained in each experiment. The rate constants for $NO_2Y^\bullet$ loss and formation of the new radical were analyzed by fitting to eq 2 as described above.

Reaction of $Y_{122}NO_2Y$-β2 or $Y_{122}NO_2Y/Y_{356}F$-β2 with ATP, CDP, and wt-α2 or $C_{439}S$-, $Y_{730}F$-, or $Y_{731}F$-α2 Monitored by EPR Spectroscopy. [Fe(II)]$_2$-$Y_{122}NO_2Y$-β2 or $Y_{122}NO_2Y/Y_{356}F$-β2 (120 μM, 5 Fe^{II}/β2) in anaerobic 50 mM HEPES (pH 7.6, 75 μL) was mixed by hand at 4 °C with an equal volume (75 μL) of O_2-saturated (2 mM) 50 mM HEPES (pH 7.6) containing CDP (4 mM) and incubated for 10 s. This solution (150 μL, 0.8 $NO_2Y^\bullet/\beta$2) was then mixed with an equal volume (150 μL) of wt or mutant-α2 (60 μM) and ATP (6 mM) in 2× assay buffer and incubated for 20 s at 25 °C. The final reaction mixture contained 30 μM $Y_{122}NO_2Y$- or $Y_{122}NO_2Y/Y_{356}F$-β2, 30 μM wt- or mutant-α2, 3 mM ATP, and 1 mM CDP in assay buffer. The solution was transferred to an EPR tube and frozen in liquid N_2. The EPR spectrum was recorded at 77 K as described above. The subtractions were carried out with the spectrum of $NO_2Y^\bullet$ and [β-$^2H_2$]$NO_2Y^\bullet$ as described above for the RFQ experiments.

Crystallization of $Y_{122}NO_2Y$-β2, Data Collection, and Refinement. $Y_{122}NO_2Y$-β2 was crystallized under conditions similar to those reported for wt- and $Y_{122}F$-β2.[40] Crystals were grown using the hanging drop vapor diffusion method against 90−95% saturated NaCl in Tris buffer, pH 7.9. Each drop consisted of $Y_{122}NO_2Y$-β2 (10 mg/mL) in 50 mM Tris, pH 7.9, and 5% glycerol. The crystals grew within 3−4 weeks and were flash-frozen in liquid N_2 using 30% glycerol in 60−70% NaCl as cryoprotectant.

Data were collected at 100 K at the European Synchrotron Radiation Facility station ID29 (Grenoble, France). The crystals were of the space group $P6_1$, with cell axes of $a = b = 137.1$ Å and $c = 109.0$ Å, containing one β2 dimer per asymmetric unit. Data were collected to 2.2 Å resolution with 100% completion. Data processing and scaling were performed using MOSFLM/SCALA.[41] The structure was solved with rigid-body refinement in Refmac (CCP4 package)[42] using the wt-β2 structure (PDB-ID: 1AV8)[40] with all waters and metals removed. Model building was done in the program O.[43] The structure was refined to $R_{fact} = 19\%$ ($R_{free} = 22\%$).

Results

Formation of a Diferric-$NO_2Y^\bullet$ Cluster in $Y_{122}NO_2Y$-β2 and Its Characterization. We have previously reported that $Y_{122}NO_2Y$-β2 has 2.9 ± 0.2 Fe/β2 and no observable radical by EPR spectroscopy.[10] Thus, if $NO_2Y^\bullet$ is generated, it must be reduced

(40) Tong, W.; Burdi, D.; Riggs-Gelasco, P.; Chen, S.; Edmondson, D.; Huynh, B. H.; Stubbe, J.; Han, S.; Arvai, A.; Tainer, J. *Biochemistry* **1998**, *37*, 5840–5848.
(41) Leslie, A. G. W. *Joint CCP4 and ESF-EACBM Newsletter* **1992**, 26.
(42) Collaborative Computational Project, Number 4. *Acta Crystallogr. D: Biol. Crystallogr.* **1994**, *50*, 760−763.
(43) Jones, T. A.; Zou, J. Y.; Cowan, S. W.; Kjeldgaard, M. *Acta Crystallogr. A* **1991**, *47* (Pt 2), 110–119.

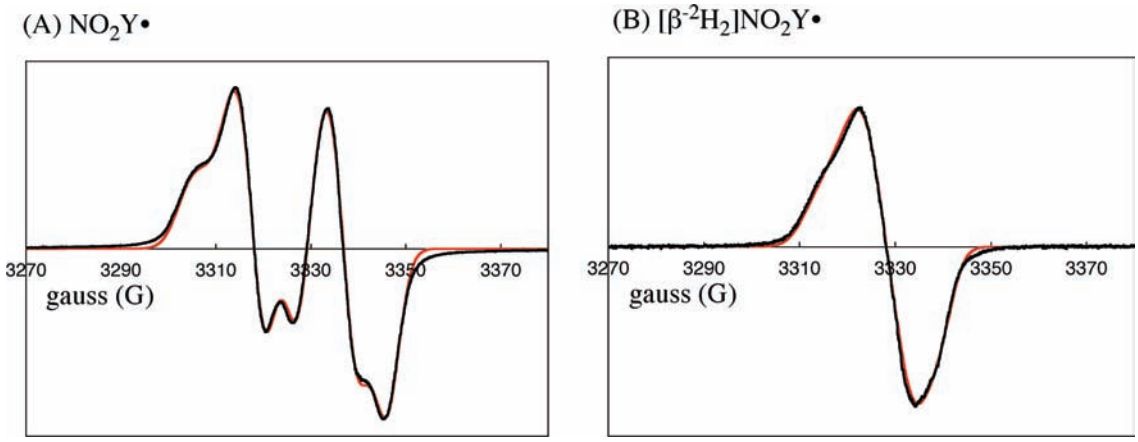

Figure 5. 9 GHz EPR spectra of (A) NO_2Y_{122}• and (B) [β-$^2H_2$]NO_2Y_{122}•. Experimental data (black trace) and simulation (red trace) are shown. The parameters used for the simulation are summarized in Table 1.

during protein purification. In a preliminary experiment, therefore, apo-$Y_{122}NO_2Y$-β2 was prepared, and the cluster was assembled at 25 °C in vitro as previously described for wt-β2.[19] The sample was frozen after 20 s incubation and analyzed by EPR spectroscopy. The results shown in Figure 5A reveal a doublet feature similar to that observed forY_{122}• in wt-β2, but with a spectral width of 64 G rather than 70 G (Figure 5A) and spin quantitation of 0.8 ± 0.05/β2. If the new radical is associated with oxidation of NO_2Y, a study of its relaxation properties will be informative, as it is located 5.0 Å from Fe1 in the diferric cluster. The power at half-saturation ($P_{1/2}$) was measured as 11.4 ± 0.5 mW at 77 K (Figure S1, Supporting Information). This value is similar to that measured for Y_{122}• in wt-β2 (28 ± 4 mW).[7] These values may be compard to the $P_{1/2}$ for the 3-aminotyrosyl radical at 730-α2 (NH_2Y_{730}•, 0.42 ± 0.08 mW[7]) and 3,4-dihydroxyphenylalanine radical at 356-β2 ($DOPA_{356}$•, 0.8 ± 0.16 mW[44]), sites further removed from the diferric cluster. This analysis suggests that the new radical is close to the diferric cluster and is likely NO_2Y•.

In general, the large doublet splitting observed for Y• in proteins is associated with hyperfine coupling with one of its two β-methylene protons.[45] Thus, to provide further support that the observed radical is located at NO_2Y, [β-$^2H_2$]NO_2Y was incorporated site-specifically into β2 (Y_{122}[β-$^2H_2$]NO_2Y-β2) and the cluster assembled. Its EPR spectrum (Figure 5B) revealed that the doublet collapsed to a broad singlet. Simulation of the spectra was carried out using EasySpin.[34] The parameters for Y_{122}• in wt-β2 were used as a starting point, excluding the hyperfine coupling associated with the proton on C3 of the ring. Least-squares fitting was performed by individually varying *g*-values, line width, hyperfine coupling constants, and Euler angles. The parameters resulting in the best fits (red overlay of experimental data in black, Figure 5) are shown in Table 1. These optimized parameters were used to simulate the data for [β-$^2H_2$]NO_2Y•, except that the ^1H hyperfine coupling constants were divided by 6.5. These results support the proposal that the species detected is the NO_2Y• and provide the standard used in the kinetic analysis described subsequently.

Maximizing NO_2Y• Formation and Determining Its Rate of Decay Using RFQ-EPR. Our previous studies on cluster assembly in wt-β2 using RFQ-EPR analysis detected an intermediate (X), an Fe^{4+}/Fe^{3+} center, that is kinetically responsible for the oxidation of Y_{122} to Y_{122}•.[16,17] Preliminary studies of cluster assembly at both 5 and 25 °C with $Y_{122}NO_2Y$-β2 suggested that an X-like species is involved in NO_2Y oxidation; however, the kinetics are complicated. The detailed analysis of this process will be reported in due course. The focus of the experiments described in this section was to maximize production of NO_2Y• formation and to determine its stability. These are essential first steps in studying the chemistry of this highly reactive, "hot" oxidant in the initiation of PCET and nucleotide reduction. In a typical experiment at 25 °C, $[Fe(II)]_2$-$Y_{122}NO_2Y$-β2 was rapidly mixed with O_2 and quenched in liquid isopentane from 0.5 to 50 s. The observed EPR signal was identical to that observed by the hand-quench experiments. No intermediate X was observed at ≥0.5 s. Each sample was analyzed by EPR spectroscopy, and the results are summarized in Figure 6. The NO_2Y• concentration is at its maximum at 1.2 ± 0.05/β2 and unchanged between 0.5 and 1 s. NO_2Y• then undergoes biexponential decay with rate constants of 0.59 s^{-1} (10%

Table 1. Parameters (in MHz) for EPR Simulation of NO_2Y• [a]

nucleus	A_{xx}	A_{yy}	A_{zz}	α	β	γ
C3,5-H	31	8.2	20	−35	12	4.7
C_β-H_a	55	46	54	0	0	0
C_β-H_b	10	13	5	0	0	0

[a] Hyperfine tensor principal values (A_{ii}) and Euler angles (α, β, γ) are indicated. The intrinsic EPR line width of 14 MHz and *g*-values of 2.00972, 2.00473, and 2.0022 were obtained from fitting.

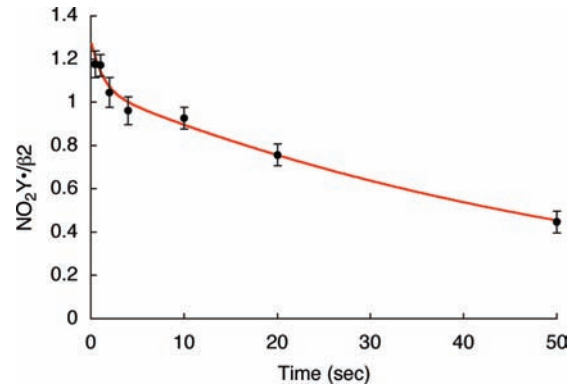

Figure 6. Generation and decay of NO_2Y_{122}•-β2 at 25 °C. The red line is a biexponential fit to the NO_2Y• reduction data with rate constants of 0.59 s^{-1} (10% amplitude) and 0.017 s^{-1} (90%).

(44) Seyedsayamdost, M. R. Ph.D. Thesis, Massachusetts Institute of Technology, 2007.
(45) Svistunenko, D. A.; Cooper, C. E. *Biophys. J.* **2004**, *87*, 582–595.

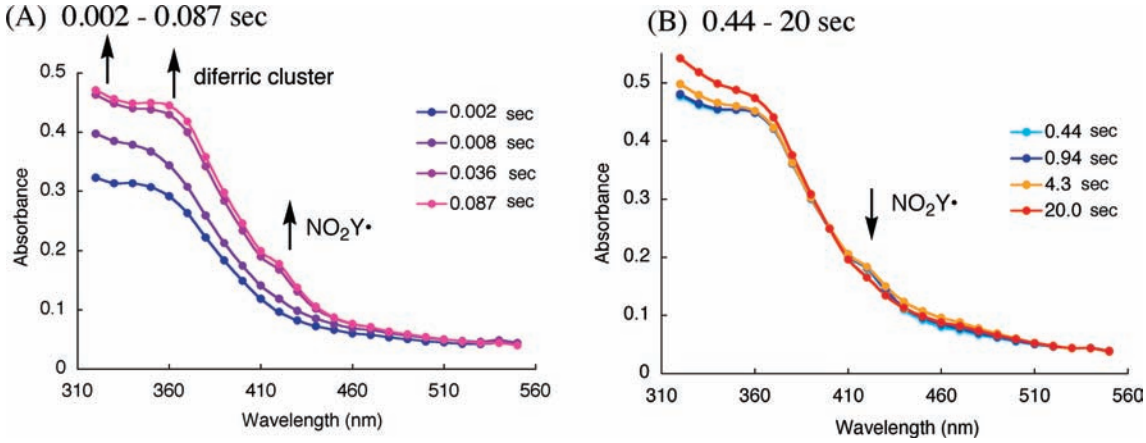

Figure 7. Point-by-point reconstruction of the absorption spectra obtained by SF UV−vis absorption spectroscopy of the reaction of $[Fe(II)]_2$-$Y_{122}NO_2Y$-$\beta2$ with O_2 to generate the $NO_2Y_{122}^{\bullet}$-$\beta2$: (A) 0.002−0.087 s and (B) 0.44−20 s at 25 °C. The lines connecting points are generated by Excel software.

amplitude) and 0.017 s^{-1} (90%), with the predominant phase giving a $t_{1/2}$ of 40 s. The amount of $NO_2Y^{\bullet}$ generated is very similar to $Y^{\bullet}$ in wt-$\beta2$, and the rate of decomposition of $NO_2Y^{\bullet}$ is sufficiently slow that mechanistic studies can be carried out.

$NO_2Y^{\bullet}$ Formation and Decay Examined by SF Spectroscopy. The absorption spectra of $NO_2Y_{122}^{\bullet}$ and $NO_2Y_{122}^{-}$ have not been reported and are required for the analysis of the kinetic studies described subsequently. The $NO_2Y^{\bullet}$ formation reaction was thus studied by SF absorption spectroscopy from 2 ms to 20 s, with each time point analyzed from 320 to 550 nm in 10 nm intervals for spectral reconstruction. A broad absorption feature at 420 nm was generated within 0.087 s and remained unchanged until 0.94 s (Figure 7A). A very small change in the 450 nm region, associated with $NO_2Y_{122}^{-}$, was observed at 4.3 s, concomitant with a decrease in the 420 nm feature (Figure 7B).

The absorption spectrum of $NO_2Y^{\bullet}$ was reconstructed from the spectrum at 0.44 s (Figure 7B). The challenging part of reconstruction is the region between 325 and 400 nm, where all the visible absorbing species contribute features. At 0.44 s, EPR studies revealed no intermediate X, and consequently no absorption feature at 365 nm associated with X, and minimal absorption at 450 nm ($\leq$0.02/$\beta2$), associated with $NO_2Y_{122}^{-}$. Thus, the predominant species at this time point are $NO_2Y^{\bullet}$, NO_2Y phenol, and the diferric cluster. Since the visible spectra of the diferric cluster and the phenol are known (Figure 4), determination of the amount of each species at this time point allows their subtraction from the composite spectrum. Our previous analysis of the isolated met-$Y_{122}NO_2Y$-$\beta2$ after in vitro cluster assembly revealed 2 diferric clusters/$\beta2$. The amount of NO_2Y phenol was estimated to be 0.8/$\beta2$, based on the amount of $NO_2Y^{\bullet}$ (1.2/$\beta2$) and total NO_2Y (2.0)/$\beta2$. After subtraction, the results reveal features at 350, 400, and 420 nm (Figure 4, green trace). The latter two features are similar to those reported for all tyrosyl radicals, including $Y_{122}^{\bullet}$ in wt-$\beta2$. $Y^{\bullet}$'s have absorption features around 410 nm with varying degrees of sharpness, with ε ranging from 3400 to 4000 M^{-1} cm^{-1}.[16,46,47] The corresponding feature of $NO_2Y^{\bullet}$ is broadened relative to that observed for $Y_{122}^{\bullet}$, and its extinction coefficient appears to be lower, $\varepsilon = 2200$ M^{-1} cm^{-1}. The feature at 350 nm is unique to $NO_2Y^{\bullet}$.

Catalytic Activity of $[NO_2Y^{\bullet}]$-$\beta2$. The generation of 1.2 $NO_2Y^{\bullet}/\beta2$ and its moderately long $t_{1/2}$ (40 s) has allowed further study of the catalytic activity of $[NO_2Y^{\bullet}]$-$\beta2$. We have previously shown that NO_2Y is 200 mV more difficult to oxidize than Y at pH 7.0[15] and blocks the PCET pathway when site-specifically incorporated in place of Y located at 356, 731, and 730 (Figure 1).[10,15] Thus, the expectation was that incubation of $[NO_2Y^{\bullet}]$-$\beta2$, a "hot" oxidant, with wt-$\alpha2$, ATP, and CDP would readily initiate radical propagation and nucleotide reduction. However, in the reverse PCET process, the pathway radical intermediates, $W_{48}^{\bullet}$ or $Y_{356}^{\bullet}$, would be unable to reoxidize NO_2Y to $NO_2Y^{\bullet}$. Whether this reaction would generate one dCDP or additional dCDPs using $W_{48}^{\bullet}$ or $Y_{356}^{\bullet}$ as new radical initiators subsequent to the first turnover is of great interest, considering our current model of radical propagation[6] and our previous and more recent observations that $[NH_2Y]$-RNRs are active.[7,48]

The activity of $[NO_2Y^{\bullet}]$-$\beta2$ was first investigated in the absence of external reductant (under single-turnover conditions) using [5-^{3}H]CDP. $[Fe(II)]_2$-$Y_{122}NO_2Y$-$\beta2$ was incubated with O_2-saturated buffer containing [5-^{3}H]CDP for 7 s at 25 °C to generate 0.95 ± 0.05 $NO_2Y^{\bullet}/\beta2$ and then mixed with wt-$\alpha2$ and ATP. A burst of 0.64 ± 0.03 equiv of dCDP was produced, followed by a slow increase in dCDP, with a rate constant of 0.004 s^{-1}, which leveled off (Figure S2, Supporting Information). The observation of 0.6 equiv of dCDPs compares to the 1.4−1.7 equiv of dCDPs produced by wt-$\beta2$ under the same conditions.[6] Inclusion of the reducing system (TR/TRR/NADPH) required for multiple turnovers did not change the size of the initial burst (Figure S2) and demonstrates that the enzyme can turnover only once with half-sites reactivity.[7,9,24,49]

The rate constant for dCDP formation was measured using the sequential mixing RCQ method (Figure 2A). $[Fe(II)]_2$-$Y_{122}NO_2Y$-$\beta2$ in anaerobic buffer was initially mixed with O_2-saturated buffer containing [5-^{3}H]CDP, and the solution was aged for 1 s at 25 °C to generate 1.2 ± 0.05 $NO_2Y^{\bullet}/\beta2$. CDP was included in this mixture to prevent turnover that can occur if $\alpha2$ contains a small amount of $\beta2$. This solution was then mixed with wt-$\alpha2$ and ATP in assay buffer and sprayed into 2% perchloric acid. The aging time after the second mixing was varied from 10 to 200 ms. The dCDP was dephosphorylated and analyzed by the method of Steeper and Steuart.[39] The results

(46) Huque, Y.; Fieschi, F.; Torrents, E.; Gibert, I.; Eliasson, R.; Reichard, P.; Sahlin, M.; Sjoberg, B. M. *J. Biol. Chem.* **2000**, *275*, 25365–25371.
(47) Thelander, M.; Graslund, A.; Thelander, L. *J. Biol. Chem.* **1985**, *260*, 2737–2741.
(48) Minnihan, E. C.; Seyedsayamdost, M. R.; Stubbe, J. Manuscript in preparation.
(49) Wang, J.; Lohman, G. J.; Stubbe, J. *Proc. Natl. Acad. Sci. U.S.A.* **2007**, *104*, 14324–14329.

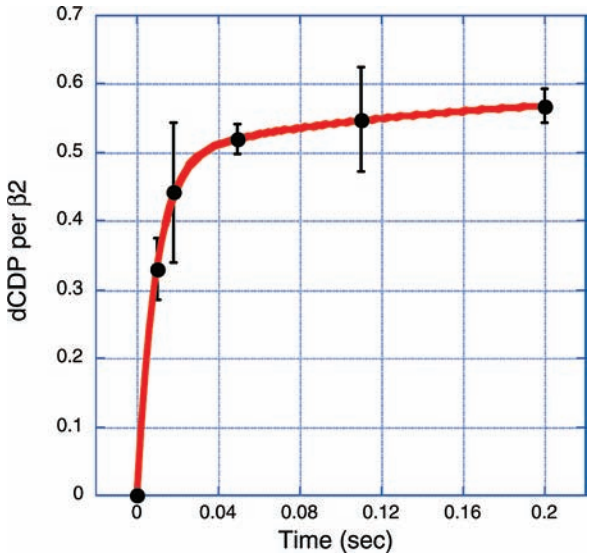

Figure 8. dCDP formation monitored by the RCQ method using sequential mixing (Figure 2A). The experiment was repeated in triplicate. The red line is a biexponential fit to the data. (See Table 2 for kinetic parameters.)

are shown in Figure 8. The data fit by eq 1 gave a rate constant for the fast phase of 107 ± 12 s^{-1} (82% amplitude) and for the slow phase of 5 ± 2 s^{-1} (18%). The total amount of dCDP formed in both phases was $0.59 \pm 0.04/\beta 2$, similar to the results described above for the hand-mixing experiments. The rate constant for dCDP formation is 10- to 50-fold faster than ever observed for wt-$\beta 2$[6] and demonstrates for the first time uncoupling between radical propagation and conformational gating. The amount of dCDP produced is one-half the amount of $NO_2Y^{\bullet}$, as observed by hand-mixing. A model (Figure 3) to explain this observation will be presented in the Discussion.

Absorption Spectrum of $NO_2Y_{122}^-$ and Kinetics of Its Formation in the Reaction of $Y_{122}NO_2Y$-$\beta 2$ with α2, ATP, and CDP Monitored by SF Absorption Spectroscopy. Because dCDP is produced, $NO_2Y^{\bullet}$ in $\beta 2$ must be reduced. The model for $Y_{122}^{\bullet}$ reduction in wt-$\beta 2$ is that it occurs by a PCET mechanism, with the proton being derived from the water on Fe1 and the electron from W_{48} or Y_{356} (Figure 1).[4,5] Since the rate-limiting step for dCDP formation catalyzed by RNR is a conformational change prior to PCET, reduction of $Y_{122}^{\bullet}$ has never been observed.[6] The rapid rate of dCDP formation suggested that we now might be able to monitor the reduction of the $NO_2Y^{\bullet}$. Since NO_2Y phenol and phenolate absorb at ~360 and 450 nm (Figure 4), respectively, the reduction of $NO_2Y^{\bullet}$ and its resulting protonation state can be investigated by SF absorption spectroscopy. As with the RCQ experiments described above, sequential mixing was used to maximize $NO_2Y^{\bullet}$ concentration. $NO_2Y^{\bullet}$ was generated from $[Fe(II)]_2$-$Y_{122}NO_2Y$-$\beta 2$ and O_2-saturated buffer containing CDP, which was further mixed with α2 and ATP (Figure 2B). Initially, a point-by-point reconstruction of the absorption spectra acquired between 2 and 180 ms was carried out to address the issue of whether the reduction gives the phenol vs phenolate. The results shown in Figure 9A reveal an increase in A_{450nm} where the $NO_2Y_{122}^-$ absorbs. The absorption spectrum of $NO_2Y_{122}^-$ was obtained by subtracting the spectrum at 2 ms from that at 120 ms (Figure 9A) in the region (430−510 nm) where spectral overlap with other species is minimal. The resulting spectrum (Figure 4, red trace) shows λ_{max} at ~450 nm, similar to that of NO_2Y^- previously observed in the $Y_{730}NO_2Y$-α2 mutant.[10] Assuming that all of the $NO_2Y^{\bullet}$ reduced, 50% of the initial $NO_2Y^{\bullet}$ determined by the RFQ experiments described subsequently, is converted to NO_2Y^-, then an ε of 6000 M^{-1} cm^{-1} can be calculated. This value is similar to the ε of NO_2Y^- previously determined for the $Y_{730}NO_2Y$-α2 mutant (6400 M^{-1} cm^{-1}).[10] Furthermore, the 50% NO_2Y^- is equivalent to the amount of dCDP measured above. These observations indicate reduction of $NO_2Y^{\bullet}$ to phenolate occurs without protonation.

A comparison of the absorption spectra of all species in the reaction mixture (Figure 4) demonstrates that formation of the NO_2Y^- can be readily monitored, with minimal interference from other species at 460 nm. Therefore, $NO_2Y_{122}^-$ formation was monitored at this wavelength (Figure 9B). The kinetic data were best fit to eq 3 with rate constants of 283 ± 25 (48% amplitude), 67 ± 3 (43%), and 10 ± 1 s^{-1} (9%), and the total change of A_{460nm} was 0.073 ± 0.003. A control in the absence of CDP revealed a very slow increase in A_{460nm} at 0.14 ± 0.02 s^{-1}. Thus, the reduction step is rapid, suggesting uncoupling of the conformational gating and multiphasic behavior, for reasons that remain to be elucidated.

Monitoring Disappearance of the $NO_2Y^{\bullet}$ and Formation of a New Radical or Radicals by RFQ-EPR Methods. The reduction of $NO_2Y^{\bullet}$ to NO_2Y^-, as well as detection of any new radicals generated as a consequence of the reduction, can be monitored by sequential mixing using the RFQ method with EPR detection. Similar to the experiments described above, 1.2 $NO_2Y^{\bullet}/\beta 2$ was generated in the presence of CDP in the first mixing event and then further reacted with α2 and ATP (Figure 2A). Time points were taken from 9 to 120 ms, and the results are shown in Figures 10 and 11. Approximately 50% of $NO_2Y^{\bullet}$ remains unchanged during the reaction, based on the stoichiometry of dCDP and NO_2Y^- formation. Thus, to facilitate the visualization of the remaining $NO_2Y^{\bullet}$ disappearance and new radical formation, 0.6 equiv of $NO_2Y^{\bullet}$ has been subtracted from each spectrum. The spectra at $t = 0$, 9, and 22 ms are shown in Figure 10 and reveal multiple species. Spin quantitation revealed no loss in radical over this time (Figure 11). Spectral overlap

Table 2. Kinetic Data for Formation of dCDP, $NO_2Y_{122}^-$, and the New Radical

		phenolate formation[a]	dCDP formation[b]	new $Y^{\bullet}$ formation[c]	$NO_2Y^{\bullet}$ decay[c]
first phase	k_{obs} (s^{-1})	283 ± 25	107 ± 12	97 ± 8	122 ± 11
	amplitude (%)	48 ± 3	82 ± 4	96 ± 3	84 ± 4
second phase	k_{obs} (s^{-1})	67 ± 3	5.3 ± 2	28 ± 7	36 ± 5
	amplitude (%)	43 ± 2	18 ± 4	4 ± 3	16 ± 4
third phase	k_{obs} (s^{-1})	10 ± 1			
	amplitude (%)	9 ± 1			
total change (/$\beta 2$)		0.61 ± 0.03[d]	0.59 ± 0.02	0.56 ± 0.04	0.56 ± 0.04

[a] Rate constants determined by SF UV−vis by monitoring changes at 460 nm. [b] Rate constants determined by RCQ. [c] Rate constants determined by RFQ-EPR. [d] $\varepsilon_{460nm} = 6000$ M^{-1} cm^{-1} was used.

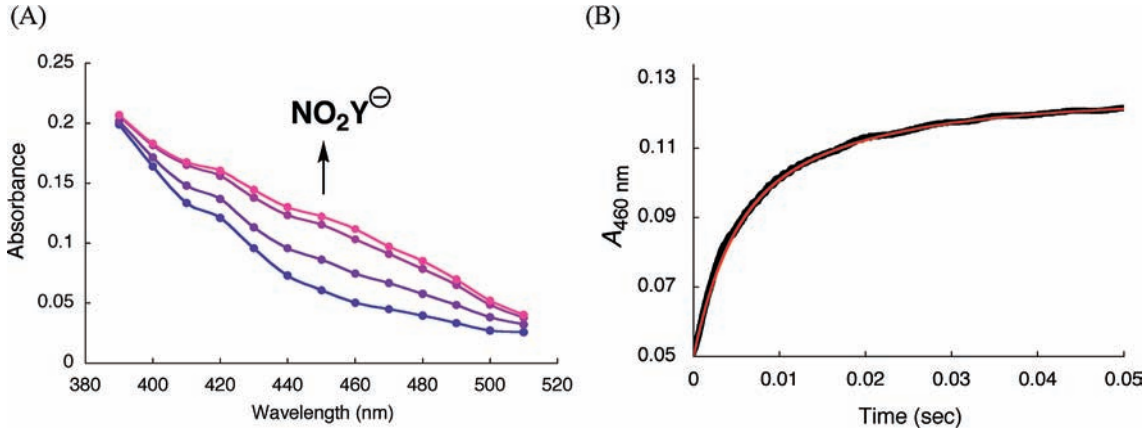

Figure 9. SF UV−vis spectroscopic analysis using sequential mixing (Figure 2B) of the reaction of $Y_{122}NO_2Y$-β2, α2, ATP, and CDP. (A) Point-by-point reconstruction of the absorption spectra between 390 and 510 nm at 2, 6, 30, and 180 ms (from blue to pink). The lines connecting the points are generated by Excel software. Each point is an average of 2−5 traces. (B) Changes in A_{460nm} (black line, an average of 15 traces). The red line is a triexponential fit (eq 3) to the data. See Table 2 for kinetic parameters.

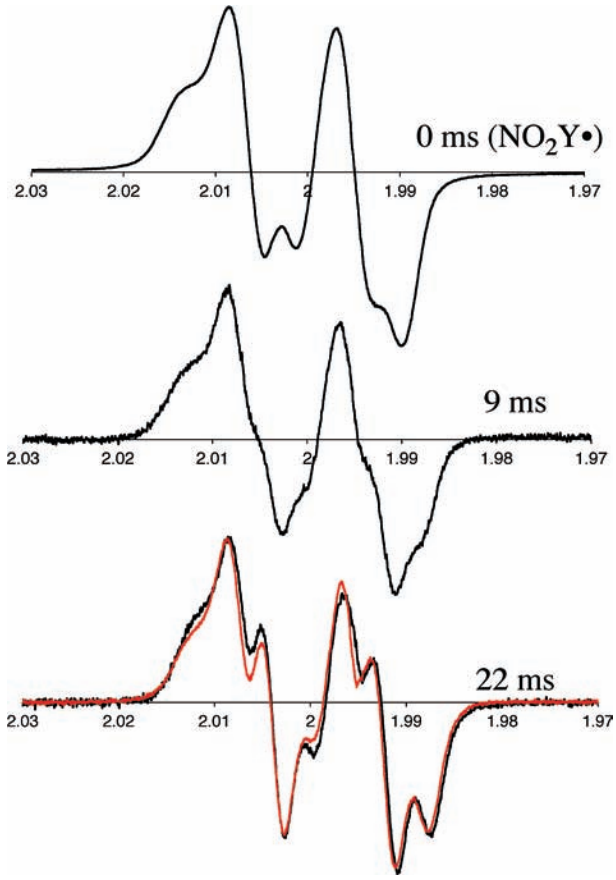

Figure 10. Time course of the reaction of $Y_{122}NO_2Y$-β2, α2, ATP, and CDP, monitored by RFQ-EPR spectroscopy (Figure 2A). Half of the concentration of the initial $NO_2Y^{\bullet}$ was subtracted from each spectrum, as 50% of the $NO_2Y^{\bullet}$ remains at the end of the overall reaction. Shown are the time points at 0, 9, and 22 ms. The red trace (bottom trace, overlaid with the 22 ms time point) is the EPR spectrum of the new radical observed by hand freeze-quench experiments (Figure S6A, Supporting Information).

of $NO_2Y^{\bullet}$ and the new radical or radicals makes analysis challenging (see Figure S3A, Supporting Information). Initially, we focused on the differences in the low-field side of the spectrum, based on an apparent peak width difference between $NO_2Y^{\bullet}$ and the new species. This method gave us an approximation of the amount of new radical (±10%). We

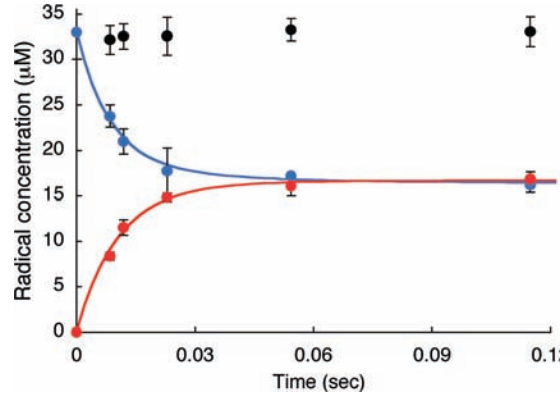

Figure 11. Time course of the experiment in Figure 10, monitored by RFQ-EPR, with total radical (black circles), $NO_2Y^{\bullet}$ (blue circles), and new $Y^{\bullet}$ (red circles). Each point represents an average of three experiments. Solid lines are biexponential fits for formation of the new $Y^{\bullet}$ and loss of the $NO_2Y^{\bullet}$. See Table 2 for the kinetic parameters.

eventually settled, however, on analyzing the reaction spectra generated with $Y_{122}NO_2Y$-β2 and Y_{122}[β-$^2H_2$]NO_2Y-β2. Our assumption was that the same species would be generated by both proteins in the same quantities. Subtractions of the $NO_2Y^{\bullet}$ spectrum and the [β-$^2H_2$]$NO_2Y^{\bullet}$ spectrum were carried out, adjusting their amplitudes to minimize differences in the spectra of the new species. One of the results using this approach is shown in Figure S3. Subtraction of $NO_2Y^{\bullet}$ (50% of the total radical, Figure S3A) and a similar experiment with [β-$^2H_2$]-$NO_2Y^{\bullet}$ (50% of the total radical, Figure S3B) from the spectrum of the 120 ms time point of each reaction resulted in very similar spectra of the new radical species (Figure S3C,D). Application of this method to the other time points (9−55 ms) revealed that the EPR spectra of the new radical species are very similar (Figure S4, Supporting Information). The amount of the new radical species formed is equivalent to the amount of $NO_2Y^{\bullet}$ lost (Figure 11). The spectrum of the new radical is also very similar to that observed by hand-quenching after incubation at 25 °C for 20 s (red trace overlaid with 22 ms spectrum in Figure 10). This new species has $t_{1/2} > 1$ min (Figure S5, Supporting Information). A power saturation experiment on the new radical revealed $P_{1/2} = 0.54 \pm 0.08$ mW (Figure S1), similar to those of $NH_2Y_{730}^{\bullet}$ (0.4 mW)[7] and $DOPA_{356}^{\bullet}$ (0.8 mW)[9] and distinct from that of $NO_2Y_{122}^{\bullet}$ (11.4 mW), suggesting that the radical is remote from the diferric cluster.

Table 3. Composition of the Radicals Observed in the Reactions of $Y_{122}NO_2Y$-β2 or $Y_{122}NO_2Y/Y_{356}F$-β2 and wt- or Mutant-α2 with ATP and CDP

	$Y_{122}NO_2Y$-β2	$Y_{122}NO_2Y$-β2/wt-α2	$Y_{122}NO_2Y/Y_{356}F$-β2/wt-α2	$Y_{122}NO_2Y$-β2/$Y_{731}F$-α2	$Y_{122}NO_2Y$-β2/$Y_{730}F$-α2	$Y_{122}NO_2Y$-β2/$C_{439}S$-α2
total radical (/β2)	0.80 ± 0.05[a]	0.60 ± 0.07	0.80 ± 0.05	0.53 ± 0.08	0.48 ± 0.06	0.52 ± 0.08
$NO_2Y^{\bullet}$ (%)	100	53 ± 3	>99	51 ± 4	60 ± 5	60 ± 5
new radical (%)	−	47 ± 3	<1	49 ± 4	40 ± 5	40 ± 5

[a] Initial $NO_2Y^{\bullet}$ before incubation with α2/ATP/CDP.

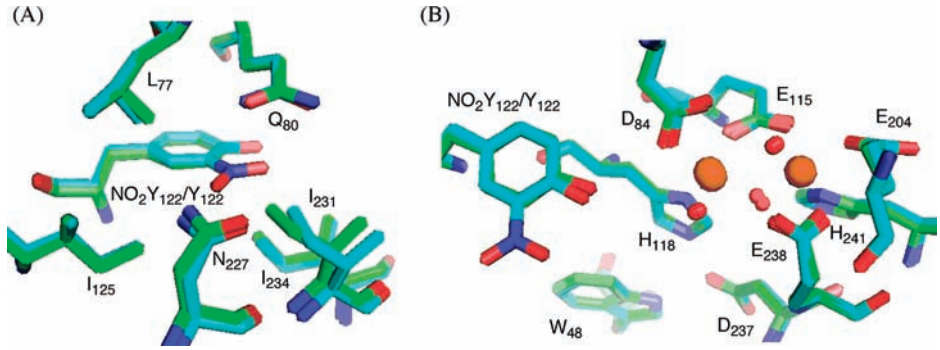

Figure 12. Overlaid crystal structures of $Y_{122}NO_2Y$-β2 (cyan) and wt-β2[50] (green, PDB-ID 1MXR), showing (A) the environment of the NO_2 group and (B) the NO_2Y-diferric cofactor. Oxygens are shown in red, nitrogens in blue, and irons in orange.

Given the single turnover for dCDP formation and the observed kinetics, the new radical (or radicals) is (are) likely to be generated in the reverse PCET process. It may be localized on W_{48}- or Y_{356}-β2 or perhaps even equilibrated with the pathway tyrosines in α. A radical associated with a pathway residue has never been observed for wt-RNR under any conditions.[6,13] The location of the radical was further investigated using α2 and β2 mutants with a pathway block: $C_{439}S$, $Y_{730}F$, or $Y_{731}F$ in α2; $Y_{356}F$ in β2. It should be noted that, in these cases, in contrast with our hypothesis for the $Y_{122}NO_2Y$-β2 reaction with wt-α2, any radical(s) observed would be associated with forward PCET pathway, as the blocked residue precludes PCET to the active site. In fact, the conformations of the Y$^{\bullet}$'s could differ in the forward and reverse PCET processes, especially near the subunit interface.

Each α2 mutant was mixed with $Y_{122}NO_2Y$-β2 (0.80 ± 0.05 $NO_2Y^{\bullet}$/β2), ATP, and CDP and incubated at 25 °C for 20 s, and the sample was frozen in liquid N_2. The reaction with the wt-α2 under identical conditions gave 0.60 ± 0.07 radical/β2, with 47% new radical (Table 3, Figure 10, and Figure S6A, Supporting Information). In these hand-mixing experiments, ~25% of the total radical is lost. The total amount of radical in mutant-α2's is ~15% less than that observed with wt-α2 (Table 3), with a 1:1 ratio of the $NO_2Y^{\bullet}$ to the new radical with $Y_{731}F$ and a 3:2 ratio of $NO_2Y^{\bullet}$ to the new radical with $Y_{730}F$ and $C_{439}S$. The new radical(s) observed with $C_{439}S$ and $Y_{730}F$-α2 mutants in the forward PCET is (are) almost indistinguishable from that observed with wt-α2 in the reverse PCET, while that observed with $Y_{731}F$-α2 is distinct (Figure S6B−D). On the other hand, when the reaction between wt-α2 and $Y_{122}NO_2Y/Y_{356}F$-β2 was examined, only $NO_2Y^{\bullet}$ was observed, 0.80 ± 0.05 equiv/β2, revealing stabilization relative to the wt- and mutant-α2's (Table 3). These observations suggest that the new radical resides primarily on Y_{356}. Further analysis is required to establish whether the observed signal contains contributions from other radicals. The minimal loss of radical in $Y_{122}NO_2Y/Y_{356}F$-β2 suggests that the 25−40% radical loss during the 20 s incubation likely occurs through a specific pathway involving Y_{356}-β2.

Structure of Met-$Y_{122}NO_2Y$-β2. Met-$Y_{122}NO_2Y$-β2 was crystallized under conditions similar to those previously described for $Y_{122}F$-β2.[40] One β2 dimer was found in the asymmetric unit. The overall structure shows minimal perturbations relative to the 1.4 Å structure of wt-β2,[50] with an rmsd of 0.3 Å for Cα in residues 10−335 of the dimer (Figure 12). The phenyl ring of NO_2Y overlays that of Y_{122} in wt-β2. The NO_2 group is parallel to the phenyl ring, on the side away from D_{84} embedded within a hydrophobic pocket composed of L_{77}, Q_{80}, I_{125}, N_{227}, I_{231}, and I_{234}-β2 (Figure 12A). One of the noticeable changes relative to the wt structure is that I_{231} within this pocket has moved 0.6−0.8 Å from NO_2Y_{122} relative to Y_{122} in wt-β2. On the other hand, the residues in the first and second coordination spheres of the diferric cluster overlay with an rmsd of 0.3 Å with the wt-β2 structure[50] (Figure 12B). In both structures, D_{84}, which may facilitate oxidation of Y_{122}, is oriented similarly, with monodentate coordination to Fe1. The mutant structure demonstrates that there are no major perturbations relative to the wt-β2 crystallized under similar conditions. However, the rates of PCET processes can be sensitive to tenths of an angstrom in donor−acceptor separation, as discussed subsequently, and the positioning of the NO_2 group may preclude the movement of this residue required for the coupling of electron and proton transfers.

Discussion

NO_2Y at position 122 in β2 has proven to be an informative probe of the radical initiation process in *E. coli* RNR. An important observation (data not shown) is that intermediate X, an Fe^{4+}/Fe^{3+} cluster involved in Y_{122} oxidation in β, is able to oxidize NO_2Y_{122} to $NO_2Y_{122}^{\bullet}$ and that the latter is sufficiently long-lived to allow its chemistry to be examined. The kinetic details of the formation of X, its characterization by EPR and Mössbauer spectroscopies, and its ability to oxidize NO_2Y_{122} will be the subject of a future report. For the present work, the conditions to maximize $NO_2Y^{\bullet}$ formation and its lifetime were established. The formation of the $NO_2Y^{\bullet}$ was detected by both EPR spectroscopy (Figure 5) and absorption spectroscopy

(50) Högbom, M.; Galander, M.; Andersson, M.; Kolberg, M.; Hofbauer, W.; Lassmann, G.; Nordlund, P.; Lendzian, P. *Proc. Natl. Acad. Sci. U.S.A.* **2003**, *100*, 3209–3214.

(Figure 7). The EPR spectrum showed a doublet feature arising from hyperfine interactions with one of the two β protons of tyrosine. The magnitude of this interaction is very similar to that observed for $Y_{122}^{\bullet}$. Incorporation of β-^{2}H-labeled NO_2Y into β2 changed the doublet hyperfine to a triplet that appears as a singlet, establishing the identity of the radical. While the visible spectrum looks like that typical of $Y^{\bullet}$ (Figure 4), the ε at 420 nm is substantially diminished relative to those of other $Y^{\bullet}$'s[16,46,47] and has an absorption feature at 350 nm that is absent in the spectra of $Y^{\bullet}$'s. Efforts to further characterize this radical with model systems and computations and by high-field EPR spectroscopy are in progress.

A number of surprises were encountered while examining the chemistry initiated by this radical. The first surprise was that $NO_2Y^{\bullet}$ reduction in the presence of α2, CDP, and ATP resulted in production of the NO_2Y^- and not the phenol. This result was unexpected for a number of reasons. First, the pK_a of NO_2Y could not be measured in holo-β2 or in the $\alpha2\beta2$ complex and must be >9.6.[10] Second, the reduction of $Y_{122}^{\bullet}$ in the wt-β2 presumably involves transfer of both an electron and a proton, although its reduction and re-oxidation have never been detected with wt-RNR due to the conformational gating.[6] Third, the structure of this mutant is similar to that of wt-β2 (Figure 12) in the first and the second coordination spheres around the diferric cluster. Finally, there is no residue in the vicinity of NO_2Y other than the putative hydroxide bound to Fe1 to pick up the proton during its oxidation.

A number of possible models are under consideration to explain the inability of the mutant to transfer a proton to $NO_2Y_{122}^-$ to regenerate the NO_2Y phenol. This observation is unusual, given that the pK_a of this residue in the met-form is so perturbed that we have been unable to detect NO_2Y^- formation by pH titration of the phenol.[10]

One possible model is that, during NO_2Y oxidation, the proton from the phenol is transferred to a position in the cluster other than the putative HO ligand on Fe1 of the intermediate X. Analysis of the structure suggests that there are no amino acid side chains positioned to accept a proton or water networks with access to the solvent. The kinetics of $NO_2Y_{122}^{\bullet}$ generation by intermediate X are complex relative to $Y_{122}^{\bullet}$ formation, and thus it is possible that the mechanism of $NO_2Y^{\bullet}$ formation is different from that for $Y^{\bullet}$. Detection of differences from the wt oxidation mechanism will require extensive RFQ spectroscopic analyses.

A second possible model is that the NO_2 group perturbs the environment of NO_2Y_{122} and/or the cluster sufficiently that the subtle conformational change(s), required for proton transfer in the forward radical propagation step, are distinct from the reverse process. Changes on the order of tenths of an angstrom are likely to be sufficient to alter proton tunneling in the PCET step.[5,12] Recent evidence detecting a subtle perturbation of the active cofactor (diferric-$Y^{\bullet}$) relative to the cofactor with the $Y^{\bullet}$ reduced is provided by comparison of the distance and orientation between Y_{122} and Fe1 in a high-resolution structure of β2 (1.4 Å) with the results from high-field EPR measurements made on the $Y_{122}^{\bullet}$ generated in the same crystal. Comparison of the orientation of the oxidized and reduced Y_{122}[50] revealed a significant rotation of the Y side chain away from the iron cluster (~1 Å). Recent FT-IR studies have also identified subtle conformational changes at peptide bonds adjacent to $Y_{122}^{\bullet}$.[51] The structure of $Y_{122}NO_2Y$-β2 indicates that I_{231} in the vicinity of NO_2Y moves substantially relative to Y in the wt-β2. It is unclear, however, how this change could translate into proton uncoupling. Although the mechanism of the mutant's inability to protonate NO_2Y is still unclear, this PCET uncoupling and the higher reduction potential of NO_2Y over Y (200 mV at pH 7.0) allows ET without the slow conformational gating (2−10 s^{-1}) observed with the wt enzyme. Thus, the chemistry of radical propagation can be investigated.

Kinetic analysis of $NO_2Y_{122}^{\bullet}$ reduction reveals that NO_2Y^- formation occurs with rate constants of 283 and 67 s^{-1} (Table 2). The rate constants are 28 and 6 times faster, respectively, than the turnover number of the wt-RNR, and the reaction occurs in two phases of almost equal amplitude. Similar "half-site" changes have now been observed with mechanism-based inhibitor studies[24,49] and with studies of radical formation with NH_2Y[7,48] and DOPA[9] analogues site-specifically incorporated into both subunits of RNR. These observations are indicative of the incompletely understood complexities in RNR's conformation and quaternary structure, which we are actively investigating.

Since $NO_2Y_{122}^{\bullet}$ is reduced, an amino acid in the pathway must be oxidized, which in turn initiates dNDP formation. Thus, dCDP formation was investigated by RCQ methods, and the formation of new radical(s) was investigated by RFQ-EPR methods. Oxidation of C_{439} to $C_{439}^{\bullet}$ is expected to be a slow step in forward radical propagation, given the redox mismatches, and thus one might expect to see an amino acid radical ($Z^{\bullet}$) transiently formed before nucleotide reduction (Figure 3). The RCQ data (Figure 8) were fit predominantly to a single exponential with $k_{obs} = 107$ s^{-1} (Table 2). However, the method of quenching (Figure 2A) limits data acquisition between 2 and 15 ms, and thus faster rate constants are not measurable. As indicated in Figure S7A in the Supporting Information (red line), a similar fit to the experimental data for dCDP production is, in fact, obtained if the rate constants and amplitudes obtained from analysis of the SF experiments for NO_2Y^- formation are used. Thus, mixing on a faster time scale is essential to tell if an intermediate radical in the forward pathway ($Z^{\bullet}$, Figure 3) could build up and actually be detected. It is interesting to note that the rate constant of ~100 s^{-1} for dCDP formation is very similar to the rate constant of 55 s^{-1} measured for the adenosylcobalamin class II RNR for dNTP formation.[52] Thus, this number may be close to the intrinsic rate constant for the chemical reduction process.

As can be seen in Figure 10, analysis by RFQ-EPR methods reveals formation of a new radical(s) within the 9 ms quench time, and $NO_2Y^{\bullet}$ appears to have been predominantly reduced by 22 ms. Recall that in all of our experiments, 50% of the $NO_2Y^{\bullet}$ remains unchanged during the time course. Thus, in all the spectra shown in Figure 10, this amount of $NO_2Y^{\bullet}$ has been subtracted to facilitate detection of spectral changes. The similarity in the widths of the EPR spectra of $NO_2Y^{\bullet}$ and the new radical(s), as noted in detail in the Results, makes it challenging to carry out subtractions required for kinetic analysis. However, the kinetics with a limited number of data points reveal that $NO_2Y^{\bullet}$ disappears with $k_{obs} = 122$ s^{-1} and that the new radical(s) appears at 97 s^{-1}. This method, as with the RCQ method, suffers from our inability to obtain data at fast enough mixing times to measure rate constants of 300 s^{-1}. Superposition of theoretical traces corresponding to the rate

(51) Offenbacher, A. R.; Vassiliev, I. R.; Seyedsayamdost, M. R.; Stubbe, J.; Barry, B. A. *J. Am. Chem. Soc.* **2009**, *131*, 7496–7497.

(52) Licht, S. S.; Lawrence, C. C.; Stubbe, J. *J. Am. Chem. Soc.* **1999**, *121*, 7463–7468.

constants and amplitudes for NO_2Y^- formation extracted from the stopped-flow absorption experiments onto the RFQ-EPR and RCQ data (Figure S7B) shows that an initial rapid phase in the latter experiments cannot be ruled out. Recent studies suggest that mixing on the 100 μs time scale will facilitate analysis of forward radical propagation.[53]

In each of the experiments described above, the amount of $NO_2Y_{122}^-$, dCDP, and new radical detected is about one-half the amount of $NO_2Y^\bullet$ at the beginning (1.2 radicals/β2) of the reaction. As noted above, this ~50% is observed repeatedly with a number of very different types of experiments. A variety of biophysical experiments are in progress to try to understand the basis for these observations. An added complication is that in β2 with 1.2 $Y^\bullet$, no one understands how the radicals are distributed between the two β monomers.

The observation that a new radical(s) builds up rapidly with a rate constant similar to that for dCDP formation suggests that it might reside on a residue in the PCET pathway including the tryptophan radical or radical cation [$W_{48}^\bullet$ or $W_{48}^{\bullet+}$] or $Y_{356}^\bullet$. The radical could, in fact, also be a composite of radicals distributed between α and β. Sequential mixing SF to look for a $W_{48}^\bullet$ (or $W_{48}^{\bullet+}$) failed to reveal any new absorption features between 510 and 560 nm,[54] a spectroscopically clean window (Figure 4). While our previous studies[55] and those of the Bollinger/Krebs groups[56,57] have established that a $W_{48}^{\bullet+}$ is involved in the diferric-$Y^\bullet$ cluster assembly, there is currently no support for or against its role in the radical propagation pathway in the class Ia RNR. Our inability to detect this radical in the double mutants suggests that its redox potential is not dramatically perturbed relative to that measured for tryptophan that is esterified and acylated in solution.[58] Thus, our favored model, based on the kinetic analyses and the preliminary studies with pathway mutants ($Y_{356}F$, $Y_{731}F$, $Y_{730}F$, and $C_{439}S$), has the new radical predominantly localized on Y_{356}.

For the first time with the *E. coli* class Ia RNR, conformational gating has been uncoupled from the chemistry. The question remains, however, as to whether it has been completely uncoupled. If we could incorporate F_3Y[59] in place of the pathway Y's, for example, we could now, by modulating the pH, determine if the rate constants we are measuring are in part or totally associated with the ET steps. In addition, experiments conducted in D_2O or at varying temperatures might allow us to determine if the rate constants we are measuring are associated with PCET. Both NO_2Y- and NH_2Y-substituted RNRs, despite the perturbation of the 3-substitutent, are starting to unveil the chemical mechanism of a very unusual and important reaction in biology. Studies in the immediate future should allow us to tell if unnatural amino acids are the perturbants we need to unravel in detail the mechanisms of PCET in RNRs.

Acknowledgment. This work was supported by NIH grant GM29595 to J.S.

Supporting Information Available: Microwave power saturation behavior of $NO_2Y^\bullet$ and new radical EPR signals; dCDP formation by $Y_{122}NO_2Y$-β2 under steady state or single turnover conditions; EPR spectra of $Y_{122}NO_2Y$-β2 and $Y_{122}[\beta$-$^2H_2]NO_2Y$-β2 incubated with wt-α2, ATP, and CDP; EPR spectra of the new radical species at time points between 9 and 55 ms; stability of new radical species; EPR spectra of the new radical species in pathway mutants; triexponential fitting of RCQ and RFQ-EPR data. This material is available free of charge via the Internet at http://pubs.acs.org.

JA1069344

(53) Yu, M. A.; Egawa, T.; Yeh, S. R.; Rousseau, D. L.; Gerfen, G. J. *J. Magn. Reson.* **2010**, *203*, 213–219.
(54) Solar, S.; Getoff, N.; Surdhar, P. S.; Armstrong, D. A.; Sing, A. *J. Phys. Chem.* **1991**, *95*, 3639–3643.
(55) Bollinger, J. M.; Tong, W. H.; Ravi, N.; Huynh, B. H.; Edmonson, D. E.; Stubbe, J. *J. Am. Chem. Soc.* **1994**, *116*, 8024–8032.
(56) Baldwin, J.; Krebs, C.; Ley, B. A.; Edmondson, D. E.; Huynh, B. H.; Bollinger, J. M. *J. Am. Chem. Soc.* **2000**, *122*, 12195–12206.
(57) Krebs, C.; Chen, S.; Baldwin, J.; Ley, B. A.; Patel, U.; Edmondson, D. E.; Huynh, B. H.; Bollinger, J. M. *J. Am. Chem. Soc.* **2000**, *122*, 12207–12219.
(58) Tommos, C.; Skalicky, J. J.; Pilloud, D. L.; Wand, A. J.; Dutton, P. L. *Biochemistry* **1999**, *38*, 9495–9507.
(59) Seyedsayamdost, M. R.; Reece, S. Y.; Nocera, D. G.; Stubbe, J. *J. Am. Chem. Soc.* **2006**, *128*, 1569–1579.